*Kinetics and Catalysis, Vol. 46, No. 1, 2005, pp. 114–122. Translated from Kinetika i Kataliz, Vol. 46, No. 1, 2005, pp. 122–130.*


# Formation of Small Rhodium Metal Particles on the Surface of a Carbon Support

**A. Yu. Stakheev[1], O. P. Tkachenko[1], K. V. Klement'ev[2, 3], W. Grünert[2], G. O. Bragina[1], I. S. Mashkovskii[1], and L. M. Kustov[1]**

[1] *Zelinskii Institute of Organic Chemistry, Russian Academy of Sciences, Moscow, 119991 Russia*
[2] *Ruhr University Bochum, D-44780 Bochum, Germany*
[3] *HASYLAB at DESY, D-22607 Hamburg, Germany*

Received November 4, 2003

**Abstract**—A rhodium catalyst supported on a Sibunit graphitized carbon carrier was studied by *in situ* XAFS spectroscopy. A comparative study of the reduction of rhodium was performed for the following two samples: Rh/C(120) dried at 120°C and Rh/C(350) calcined at 350°C. EXAFS data showed an absence of carbon atoms within the nearest environment of rhodium atoms in the Rh/C(120) uncalcined sample, which implies the absence of direct interaction between rhodium and the carbon support. In the course of the reduction of this sample (200°C), coarse particles with small metal cores were initially formed. These metal particles rapidly agglomerated upon the complete reduction of rhodium (350°C). These reduction of the Rh/C(350) calcined sample at 100–500°C resulted in the formation of small metal particles early in the reduction (100°C). The high dispersity of these particles was retained as the temperature of treatment in hydrogen was increased to 500°C due to metal–support interaction. The conversion of benzene into cyclohexane on the Rh/C(350) catalyst containing small rhodium particles was much higher at the same temperature of hydrogenation.

## INTRODUCTION

Like commonly used supports, such as oxides and zeolites, carbon supports exhibit a developed surface and porosity; because of this, they can be widely used in catalysis. Moreover, corrosion resistance and cost factor are among the advantages of a carbon support over acid and base supports.

Carbon-supported metals are used as catalysts in the small-scale commercial production of pure organic chemicals and in the large-scale production of polymers [1]. A study of Rh-containing catalysts is of particular interest because homogeneous rhodium complexes are widely used in industrial olefin hydroformylation [2] and in the production of acetic acid [3].

Attempts at using heterogeneous analogs in methanol carbonylation demonstrated that carbon-supported catalysts exhibit high activity and selectivity in the formation of acetic acid [4–7]. Moreover, a rhodium catalyst supported on carbon was found to be active in hydrogenation [8–11], hydrogenolysis [12], isomerization [11, 13], chlorine removal from chlorine-containing wastes [14, 15], and ammonia synthesis [16]. This catalyst was studied in most detail in the carbonylation reactions of olefins and alcohols [5, 17–26].

It was found that the activity and selectivity of an Rh/C catalyst essentially depend on the size of rhodium particles [11, 17–20, 24]. Skell and Ahmed [11] found that the selectivity of low-percentage (0.02 wt %) catalysts containing monatomic ($Rh_1$) and diatomic ($Rh_2$) active centers for *cis*-2-butene in the hydrogenation of 1,3-butadiene was higher by one order of magnitude than that of a 1% Rh/C catalyst containing bulky metal particles.

In turn, Halttunen and coauthors [17, 18] described 5–7% Rh/C catalysts with finely dispersed rhodium particles on a mesoporous carbon support containing thermally stable oxygen-containing groups in a sufficiently high concentration. In a study of methanol hydrocarbonylation on these catalysts, they found that the carbonylating activity (high selectivity for acetic acid and methyl acetate) was related to the presence of small rhodium particles, whereas the conversion of methanol into acetaldehyde and ethanol occurred on coarse rhodium particles.

The aim of this work was to develop a procedure for preparation of a catalyst containing Rh metal particles of different sizes on a Sibunit graphitized carbon support. To reduce the metal particle size, we used an adsorption method, which allowed us to reach the molecularly dispersed state of rhodium on the support surface at the stage preceding reduction. Previously [27], we found that adsorption supporting of the ammonia complexes of noble metals is best suited for the supporting of a molecularly dispersed complex (noble metal precursor) onto the carbon support.

Previously [28, 29], it was also found that calcination is required for the preparation of highly dispersed metal particles immobilized on zeolite supports when the ammonia complexes of metals are used. In the course of this calcination stage, $NH_3$ ligands are

0023-1584/05/4601-0114 © 2005 MAIK "Nauka/Interperiodica"

removed. To clarify the effect of this factor on the size of rhodium particles immobilized on Sibunit and on the resistance of these particles to agglomeration, the catalyst was treated in air at different temperatures (120 and 350°C) before reduction. In this case, it was assumed that, as a result of sample treatment in air at a low temperature (120°C), the ammonia complex of rhodium underwent only partial degradation.

The extent of rhodium reduction and the structure of metal particles were monitored by measuring XAFS spectra. The catalytic activity of Rh/C catalysts was studied using a model structure-insensitive reaction of benzene hydrogenation as an example.

## EXPERIMENTAL

**Catalyst preparation.** A 0.5- to 1.0-mm fraction of Sibunit graphitized carbon support, which had been prepared at the Boreskov Institute of Catalysis, Siberian Division, Russian Academy of Sciences (Novosibirsk), was used for preparing the 2% Rh/C catalyst. The support surface was preoxidized by treatment with a 0.2 M $KMnO_4$ solution followed by washing with a 4 N HCl solution. The activation procedure was described in more detail elsewhere [27]. Rhodium was supported by ion exchange from an aqueous solution of the ammonia complex $[Rh(NH_3)_5Cl]Cl_2$ at room temperature with continuous stirring for 3 h. After washing the Rh/C sample to a neutral pH value, it was divided into two portions. One portion of the sample (Rh/C(120)) was dried in a drying oven at 120°C, and the other portion (Rh/C(350)) was calcined in a flow of air at 350°C for 3 h. The specific surface areas of the dried and calcined samples were 317 and 279 $m^2/g$, respectively, as determined by the BET method from nitrogen desorption data.

**XAFS spectra.** The XAFS spectra were measured at the X1 EXAFS station in the HASYLAB laboratory at the Deutsches Elektronen-Synchrotron in der Helmholtz-Gemeinschaft DESY (Germany). The primary X-ray beam was monochromated using a (+/–) double crystal Si(311) monochromator. The ionization chambers were filled with optimum gases for rhodium *K*-edge measurements: the first chamber was filled with argon (~1000 mbar), and the second and third chambers were filled with krypton (~800 mbar). The spectra were measured in a transmission mode at liquid nitrogen temperature in flowing helium. The spectra were recorded at a constant photon-energy step $\Delta E = 0.2$ eV in the XANES region and at a constant step $\Delta k = 0.025$ Å$^{-1}$ of the photoelectron wave vector in the EXAFS region.

All of the spectra were measured two or three times in order to reach the required reproducibility and statistics. The *in situ* reduction of samples was performed in a special chamber designed at Utrecht University (the Netherlands) [30]. For the reduction of catalysts, a gas mixture containing 5 vol % $H_2$ in He was used, which was supplied to the EXAFS cell through a purification system. Catalyst pellets were pressed into a chuck. Rhodium foil was used as a reference substance.

The EXAFS spectra were calculated with the use of VIPER for Windows [31]. To separate changes in photoionization due to the atom from changes due to backscattering from neighboring atoms, the EXAFS function $\chi$, which was determined from absorption coefficient $\mu$, was introduced and multiplied by $k^2$ over the wave number range 4.15–15.95 Å$^{-1}$.

To obtain quantitative information from EXAFS spectra, contributions from shells to the total signal were simulated. These contributions were separated from the total signal by Fourier transform with the use of the well-known EXAFS formula in the harmonic approximation,

$$\chi = S_0^2 \sum_j \frac{N_j F_j(k)}{kR_j^2} \exp(-2\sigma_j^2 k^2) \sin[2kR_j + \phi_j(k)],$$

which means summation over *j*th atomic shells. Here, $F$ is the backscattering amplitude and $\phi$ is the phase shift function, which were calculated with the use of the *ab initio* FEFF8.10 program [32] and checked using the EXAFS spectra of the reference Rh foil (Rh–Rh distance of 2.6894 Å; coordination number of 12).

The experimental and theoretical spectra were compared in both reciprocal (wave number) $k$ and real (coordinate) $r$ spaces. The following parameters were used for fitting theoretical spectra to experimental data: the shell radius $R_j$, the coordination number $N_j$, the Debye–Waller factor $\sigma_j^2$, and the difference between calculated and experimental absorption edge energy positions $\Delta E_j$. Errors in the fitting parameters were found by the expansion of the statistical function $\chi^2$ near its minimum taking into account maximum pair correlations.

To evaluate the formal average cluster size (particle radius ($R$, Å)) from coordination numbers and Rh–Rh distances in the first coordination sphere, which were obtained by calculating EXAFS data, the following equation was used [33]:

$$\text{c.n.}_{\text{cluster}} = \text{c.n.}_{\text{crystal}}(1 - 3/4\rho + 1/16\rho^3),$$

where $\rho = r/R$; $r$ is the Rh–Rh interatomic distance in the first shell, Å; $\text{c.n.}_{\text{cluster}}$ is the coordination number of the first shell; and $\text{c.n.}_{\text{crystal}} = 12$ for the fcc lattice of rhodium.

In addition, XANES data were used. On comparison with XANES data from Rh foil, they provide information on the electronic state of the absorbing atom, that is, on electron density distribution near the absorbing atom [34].

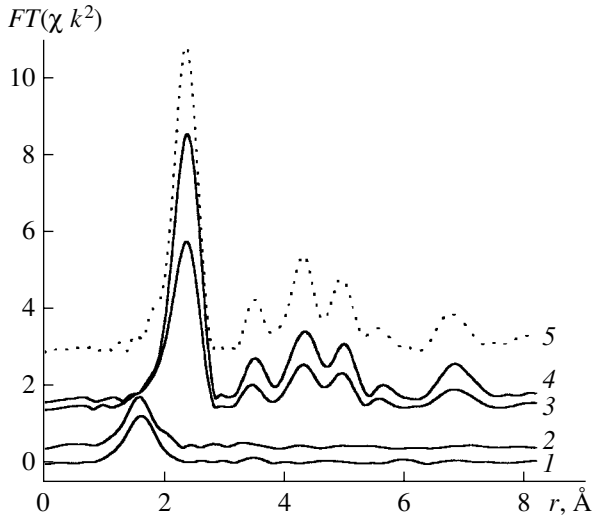


**Fig. 1.** Fourier transform of the Rh *K*-edge EXAFS spectra of (*1*) the initial Rh/C(120) sample; the Rh/C(120) samples reduced at (*2*) 150, (*3*) 200, and (*4*) 350°C; and (*5*) rhodium foil.

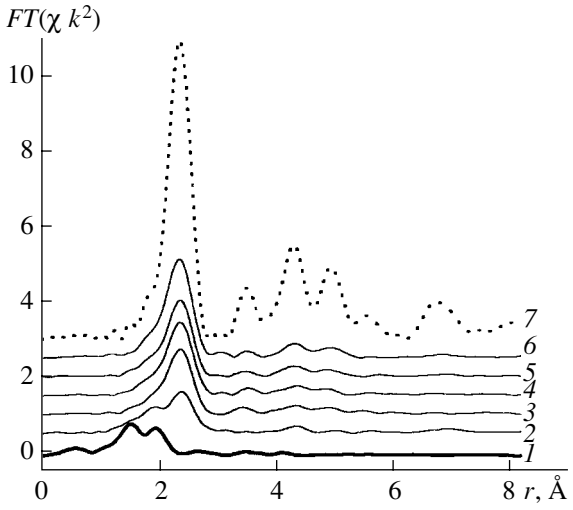


**Fig. 2.** Fourier transform of the Rh *K*-edge EXAFS spectra of (*1*) the initial Rh/C(350) sample; the Rh/C(350) samples reduced at (*2*) 100, (*3*) 200, (*4*) 300, (*5*) 400, and (*6*) 500°C; and (*7*) rhodium foil.

**Catalytic activity of Rh/C(120) and Rh/C(350).** The activity of Rh/C(120) and Rh/C(350) catalysts in benzene hydrogenation was studied in a small-volume flow reactor at atmospheric pressure over the temperature range 80–200°C. The catalysts (0.1 g of a fraction with a particle size of 0.20–0.63 mm) were loaded in the reactor. Hydrogen from a cylinder was passed through an evaporation mixer, and benzene was simultaneously supplied to this evaporator mixer. Thereafter, the mixture arrived at the heated reactor with the catalyst. The flow rates of hydrogen and benzene were 160 ml/min and 1 ml/h, respectively. The reaction products were analyzed on a Chrom-5 chromatograph equipped with a thermal-conductivity detector. The stainless-steel chromatographic column (4 m × 3 mm) was packed with 15% Carbowax 20M on Chezasorb (particle size of 0.25–0.36 mm). Helium was used as the carrier gas. The catalysts were reduced in flowing hydrogen at 350°C for 1 h before performing the hydrogenation reaction. Only cyclohexane was detected in the reaction products.

## RESULTS AND DISCUSSION

Figures 1 and 2 show radial distribution functions obtained by Fourier transform of the oscillating parts of the Rh *K*-edge EXAFS spectra of the Rh/C(120) and Rh/C(350) catalysts, respectively. For comparison, the radial distribution function for Rh foil, whose spectrum was measured under analogous conditions, is also shown in Figs. 1 and 2. Tables 1 and 2 summarize the structures of the nearest environment of the rhodium atom in the catalysts as calculated from EXAFS data. Tables 3 and 4 summarize the formal average sizes of rhodium metal clusters in Rh/C catalysts with consideration for errors.

### *Structure of the Initial Samples*

A comparison between Figs. 1 and 2 reveals a considerable difference between the spectra of the initial samples (dried Rh/C(120) and calcined Rh/C(350)). Thus, a peak with $r < 2$ Å, which corresponds to the occurrence of lighter atoms near the absorbing rhodium atom, was detected in the spectrum of the initial dried sample. In our case, these atoms may be the oxygen atoms of the carboxyl surface groups of the support, the carbon atoms of the support, or the nitrogen atoms of an ammonia complex [27]. Because the atoms (O, C, and N) are similar in atomic weight and atomic size, the X-ray scattering amplitudes and phases for these atoms are similar. Consequently, they are practically indistinguishable as scattering atoms in EXAFS spectroscopy. Nevertheless, it is believed that nitrogen atoms from the undecomposed ammonium complex of rhodium constitute at least a portion of atoms in the nearest environment of the central atom of rhodium in the sample dried at 120°C.

The EXAFS data suggest that five light atoms arranged at a distance of 2.08 Å are the nearest neighbors of the central atom of rhodium (Fig. 1, Table 1).

Unlike the spectrum of the uncalcined sample, the spectrum of the initial calcined sample exhibited two peaks. Calculation of experimental data showed the occurrence of two groups of atoms near the rhodium atom. One of these groups was at a distance of 2.07 Å, and the other was at a distance of 2.21 Å (Fig. 2, Table 2). In this case, it was found that six and four nearest neighbors occurred at the shorter and longer distances,

**Table 1.** EXAFS data obtained in the reduction of the Rh/C(120) sample

| Temperature of treatment in $H_2$, °C | Atomic pairs | $r$, Å | Coordination number | $\sigma^2 \times 10^{-3}$, Å$^2$ | $\Delta E$, eV |
|---|---|---|---|---|---|
| initial | Rh–O(N)* | 2.081(4)** | 5.2(1) | 6.8(1) | 13(1) |
| 50 | Rh–O(N) | 2.073(4) | 5.0(1) | 5.9(1) | 7(1) |
| 75 | Rh–O(N) | 2.067(4) | 5.0(1) | 5.8(1) | 8(1) |
| 100 | Rh–O(N) | 2.072(3) | 5.3(1) | 6.2(1) | 12(1) |
| 150 | Rh–O(N) | 2.079(6) | 5.2(2) | 5.9(1) | 10(1) |
| 200 | Rh–O(N) | 2.096(3) | 1.9(4) | 9.3(1) | 10(2) |
| | Rh–Rh | 2.689(3) | 6.1(3) | 2.9(1) | 0.6(6) |
| 250 | Rh–O(N) | 2.101(3) | 0.5(7) | 12.8(3) | 10(4) |
| | Rh–Rh | 2.683(3) | 9.1(5) | 2.7(1) | 0.3(6) |
| 300 | Rh–Rh | 2.684(3) | 9.6(4) | 2.9(1) | 2.5(5) |
| 350 | Rh–Rh | 2.682(2) | 10.0(4) | 2.8(1) | 5.9(4) |

* O and N are practically indistinguishable (see the text).
** Error in the last decimal place.

**Table 2.** EXAFS data obtained in the reduction of the Rh/C(350) sample

| Temperature of treatment in $H_2$, °C | Atomic pairs | $r$, Å | Coordination number | $\sigma^2 \times 10^{-3}$, Å$^2$ | $\Delta E$, eV |
|---|---|---|---|---|---|
| initial | Rh–O | 2.074(7)* | 5.8(3) | 5.1(1) | 21(1) |
| | Rh–C | 2.208(9) | 3.9(3) | 1.1(1) | 6(1) |
| 100 | Rh–C | 2.176(5) | 2.9(1) | 10.5(1) | 21(4) |
| | Rh–Rh | 2.671(3) | 2.1(1) | 4.2(3) | 3(1) |
| 150 | Rh–C | 2.165(8) | 2.0(1) | 10.9(2) | 23(6) |
| | Rh–Rh | 2.670(3) | 2.8(1) | 4.9(3) | 3(1) |
| 200 | Rh–C | 2.176(2) | 0.8(1) | 5.6(4) | 16(2) |
| | Rh–Rh | 2.683(4) | 3.7(2) | 5.3(4) | 0.4(4) |
| 250 | Rh–C | 2.176(3) | 0.8(1) | 5.6(4) | 16(2) |
| | Rh–Rh | 2.684(3) | 4.3(2) | 5.3(4) | –2.1(4) |
| 300 | Rh–C | 2.179(2) | 0.7(1) | 7.7(4) | 16(2) |
| | Rh–Rh | 2.672(2) | 4.5(1) | 5.7(2) | –1.7(2) |
| 350 | Rh–C | 2.199(3) | 0.6(1) | 9.4(9) | 29(3) |
| | Rh–Rh | 2.668(3) | 4.5(2) | 5.3(3) | 0.1(3) |
| 400 | Rh–C | 2.197(2) | 0.5(1) | 2.3(4) | 21(2) |
| | Rh–Rh | 2.678(3) | 4.3(1) | 5.1(3) | –0.9(3) |
| 450 | Rh–C | 2.188(2) | 0.4(1) | 2.6(2) | 21(2) |
| | Rh–Rh | 2.673(1) | 4.7(1) | 5.1(1) | –2.5(2) |
| 500 | Rh–C | 2.194(3) | 0.3(1) | 0.8(6) | 19(5) |
| | Rh–Rh | 2.678(2) | 5.2(2) | 4.7(2) | –3.6(3) |

* Error in the last decimal place.

**Table 3.** Average formal diameters of rhodium metal clusters in the reduced Rh/C(120) sample according to EXAFS data

| Reduction temperature, °C | Rh–Rh distance, Å | Coordination number | Average diameter of Rh particles, Å |
|---|---|---|---|
| 200 | 2.689 ± 0.003 | 6.1 ± 0.3 | 7.9* ± 0.5 |
| 250 | 2.683 ± 0.003 | 9.1 ± 0.5 | 16.5 ± 3.5 |
| 300 | 2.684 ± 0.003 | 9.6 ± 0.5 | 20.0 ± 5.3 |
| 350 | 2.682 ± 0.002 | 10.0 ± 0.4 | 24.0 ± 6.1 |

* The formal average diameter of the metal core of a rhodium particle.

**Table 4.** Average formal diameters of rhodium metal clusters in the reduced Rh/C(350) sample according to EXAFS data

| Reduction temperature, °C | Rh–Rh distance, Å | Coordination number | Average diameter of Rh particles, Å |
|---|---|---|---|
| 100 | 2.671 ± 0.003 | 2.1 ± 0.1 | 4.2 ± 0.1 |
| 150 | 2.670 ± 0.003 | 2.8 ± 0.1 | 4.6 ± 0.1 |
| 200 | 2.683 ± 0.004 | 3.7 ± 0.2 | 5.3 ± 0.2 |
| 250 | 2.684 ± 0.003 | 4.3 ± 0.2 | 5.8 ± 0.2 |
| 300 | 2.672 ± 0.002 | 4.5 ± 0.1 | 6.0 ± 0.1 |
| 350 | 2.668 ± 0.003 | 4.5 ± 0.2 | 6.0 ± 0.2 |
| 400 | 2.678 ± 0.003 | 4.3 ± 0.2 | 5.8 ± 0.2 |
| 450 | 2.673 ± 0.001 | 4.7 ± 0.1 | 6.2 ± 0.1 |
| 500 | 2.678 ± 0.002 | 5.2 ± 0.2 | 6.7 ± 0.2 |

respectively. At first glance, it may seem improbable that ten light atoms occur in the nearest environment of the rhodium atom. However, indeed, six oxygen atoms and four carbon atoms occur in the first and second coordination spheres of rhodium, respectively, if we assume that the rhodium atom is coordinated to three carboxyl groups and one carbon atom of the support. The replacement of O atoms by C atoms in the first coordination sphere of the Rh atom changes the coordination number because the scattering amplitude of the Rh–O pair is greater (by ~40%) than that of the Rh–C pair. An increase in the coordination number of the first coordination sphere from 6 to 8 suggests that this version is less plausible.

We can conclude that oxygen and carbon atoms are the nearest neighbors of the rhodium atom in the calcined Rh/C(350) sample because treatment in air at 350°C results in the complete degradation of the ammonia complex of rhodium. In this case, it is reasonable to assume that the oxygen atoms of oxygen-containing surface groups, at which rhodium is immobilized, occur at a shorter distance from the rhodium atom, whereas the carbon atoms of the support occur at a longer distance. Pinxt *et al.* [35] came to an analogous conclusion on the coordination of Pt to graphite via oxygen; based on EXAFS data, the values of 2.03 and 2.62 Å were attributed to the Pt–O and Pt–C distances, respectively. In other publications [36, 37], where the modification of carbon fibers with Rh-containing complexes and the structure of small rhodium metal particles immobilized on carbon fibers were studied, 2.05 and 2.25 Å were attributed to the Rh–O/N and Rh–C distances, respectively. Note that the Rh–O distance in $Rh_2O_3$ is equal to 2.05 Å, and the coordination number is 6 [38].

The fact that distances to the nearest light atoms were equal in both of the samples (2.07 and 2.08 Å) suggests that, in the case of incomplete degradation of the ammonia complex, nitrogen atoms either did not occur in the nearest environment of the rhodium atom or, most likely, occurred at the same distance from it as oxygen atoms.

Figure 3 demonstrates the Rh *K*-edge XANES spectra of the initial Rh/C(120) and Rh/C(350) samples and Rh foil. A shift of the peak of the Rh *K*-edge to higher photon energies, as compared with the position of the absorption edge characteristic of the spectrum of bulk metal (23220 eV), is indicative of the occurrence of a positive charge on the absorbing atom of Rh. This shift in the peaks of the Rh *K*-edge was found in both of the initial samples. However, note that this shift in the spectrum of the Rh/C(120) sample was more significant than that in the spectrum of the Rh/C(350) sample. The difference in the effective positive charges on the absorbing atom of Rh and the fact that the average Rh–O(N) coordination numbers differ by unity in both of the samples suggest that rhodium in the calcined sample occurred in a six-coordinated state (as in $Rh_2O_3$), which is typical of trivalent rhodium. However, the presence of ammonia ligands in the uncalcined sample increased the effective positive charge on the rhodium atom.

Moreover, the intensity of the first peak after the edge ("white line"), which is related to the charge state of the absorbing atom, in the XANES spectrum of either of the samples was much higher than the corresponding line intensity in the spectrum of the bulk metal. This indicates the presence of a positive charge on rhodium atoms in both of the initial samples.

### *Reduction of the Rh/C(120) Sample*

A comparison between Figs. 1 and 2 (even without calculating the EXAFS spectra) suggests that the reduction of the two Rh/C catalyst samples pretreated under different conditions occurred in different manners. The reduction of rhodium in the sample predried at 120°C began only at 200°C in hydrogen (Fig. 1, curve *3*). This reduction occurred stepwise. At lower temperatures of treatment in hydrogen, a peak between 2 and 3 Å was almost absent from the Fourier transform

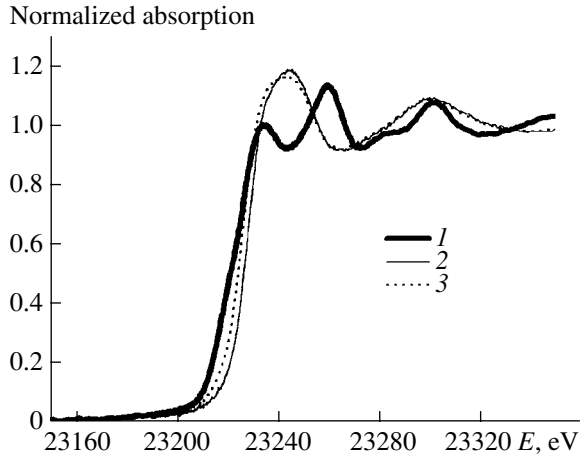


**Fig. 3.** Experimental XANES spectra of (*1*) rhodium foil and the initial (*2*) Rh/C(120) and (*3*) Rh/C(350) samples.

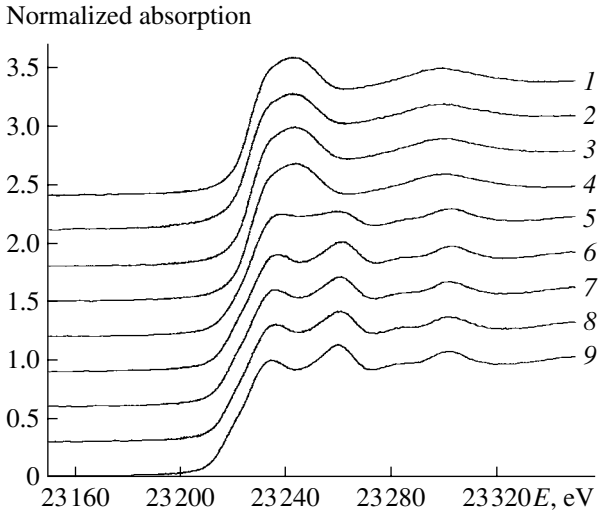


**Fig. 4.** Experimental XANES spectra of the Rh/C(120) samples reduced at (*1*) 50, (*2*) 75, (*3*) 100, (*4*) 150, (*5*) 200, (*6*) 250, (*7*) 300, and (*8*) 350°C and (*9*) rhodium foil.

curve. This suggests that the nearest environment of the absorbing atom of rhodium was free of rhodium atoms (curve *2*). Up to 200°C, the radial distribution function exhibited only one peak with $r < 2$ Å, which is analogous to the peak found in the initial unreduced sample. The quantitative analysis of EXAFS data for the Rh/C(120) sample (Table 1) shows that the distance between rhodium atoms and its nearest neighboring atoms remained almost unchanged (2.07–2.08 Å) before the onset of rhodium metal formation (~200°C). Under these conditions, the number of the nearest neighbors of the rhodium atom also remained unchanged (average coordination number of ~5).

In the course of reduction of this sample at 200°C, three of the five nearest light atoms were lost and six rhodium atoms appeared as the nearest neighbors at a distance of ~2.69 Å. After the reduction at 250°C, for each two rhodium atoms, there was only one light atom (average coordination number of 0.5). Moreover, starting at a reduction temperature of 200°C, the appearance of peaks with $r > 3$ Å can be observed in the EXAFS spectra. These peaks are analogous to the peaks observed in the spectra of rhodium foil (Fig. 1). The appearance of so-called "long-range peaks" in the spectra suggests that large metal particles began to form even at the specified temperature. Although the Rh–Rh coordination number in such a particle was found to be equal to 6.1, it should be borne in mind that this coordination number is averaged over all of the rhodium atoms, a portion of which remained bound to oxygen and/or nitrogen atoms.

The average particle size estimated from the average coordination number depends on the morphology of particles. In this case, the estimate of average particle size is very rough. Because the geometry of formed particles is unknown, we worked on the assumption that they are spherical. In such a case, it is likely that the particles consist of a metal core surrounded by charged rhodium oxide ions and/or partially decomposed rhodium ammoniate ions. Although the rhodium particle diameter was formally calculated to be ~8 Å (Table 3), we cannot conclude that highly disperse Rh particles occurred on the surface of Sibunit. To the contrary, the appearance of long-range peaks in the radial distribution curve at a distance of ~7 Å suggests that coarse rhodium particles were formed along with small particles even at the beginning of reduction of the dried Rh/C(120) sample. As the reduction temperature of this sample was further increased, the average Rh–O(N) coordination number decreased very rapidly and the average Rh–Rh coordination number gradually decreased to reach 10 at 350°C. The formal average particle diameter of rhodium metal became equal to ~24 Å.

The fact that the reduction of rhodium in this sample began only at 200°C may be supported by another portion of the XAFS spectra (XANES) shown in Fig. 4. A noticeable Rh *K*-edge shift to higher photon energies, which is indicative of the presence of a positive charge on the absorbing atom of Rh, was observed in the Rh/C(120) sample treated in a mixture of 5% $H_2$ in helium at temperatures lower than 200°C (curves *1–4*). Moreover, the intensity of the white line at the specified temperatures was much higher than that at higher reduction temperatures. The height of this line at 250–350°C was close to the height of the white line for the bulk metal (curves *5–9*).

### *Reduction of the Rh/C(350) Sample*

The reduction of the sample precalcined in air at 350°C yielded other results (Fig. 2, Table 2). Even at 100°C, the nearest neighbors at a distance of 2.07 Å (oxygen atoms) were completely removed and a light atom at a distance of ~2.2 Å (carbon atoms) was lost. At

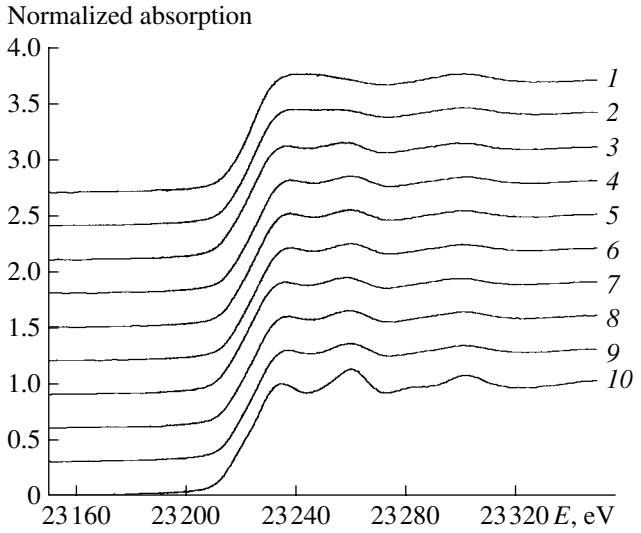


**Fig. 5.** Experimental XANES spectra of the Rh/C(350) samples reduced at (*1*) 100, (*2*) 150, (*3*) 200, (*4*) 250, (*5*) 300, (*6*) 350, (*7*) 400, (*8*) 450, and (*9*) 500°C and (*10*) rhodium foil.

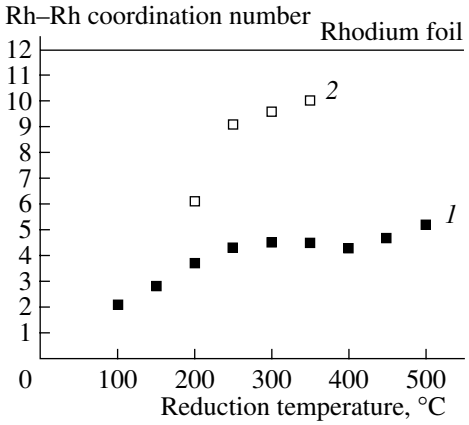


**Fig. 6.** Dependence of the Rh–Rh coordination number in the (*1*) Rh/C(350) and (*2*) Rh/C(120) samples on the temperature of reduction.

the same time, the Fourier transform curve (Fig. 2, curve *2*) exhibited a peak at a distance that corresponds to the Rh–Rh atomic pair. Thus, it is evident that the reduction of rhodium in this sample began even at 100°C in hydrogen.

This inference is supported by the XANES spectra shown in Fig. 5. An Rh *K*-edge shift to higher photon energies, which indicates that rhodium is positively charged, was observed only in the initial Rh/C(350) sample (Fig. 3, curve *3*). According to EXAFS data, six oxygen atoms are the nearest neighbors of the rhodium atom in this sample. The intensity of the white line only in the XANES spectrum of the initial sample was much higher than that in the spectra of reduced samples. As the temperature was increased, the intensity of this line approached the intensity of the white line for the bulk metal. Moreover, the presence of small metal particles was also supported by a low intensity of oscillations in the region close to the absorption edge.

As the reduction temperature was increased from 100 to 500°C, carbon atoms further disappeared from the nearest environment of the rhodium atom. At 500°C, only one carbon atom for three rhodium atoms was retained as the nearest neighbor (average coordination number of 0.3). Note that rhodium metal particles initially formed in the reduction (100°C) of the calcined Rh/C(350) sample were very small, although the presence of barely perceptible long-range peaks suggested the occurrence of an insignificant amount of relatively large particles. Under these conditions, the average Rh–Rh coordination number was equal to ~2. As the reduction temperature was further increased, the Rh–C coordination number decreased to 0.3 (500°C) and the average Rh–Rh coordination number gradually increased (to ~3, ~4, and ~5 at 150, 200–400, and 450–500°C, respectively). In this case, the average particle size of rhodium metal increased insignificantly, and the formal particle diameter reached ~6.7 Å at 500°C.

Figure 6 shows the effect of the reduction temperature of Rh/C samples on the Rh–Rh coordination number, that is, on the particle size of rhodium metal evaluated from EXAFS data. It can be clearly seen in Fig. 6 that precalcination should be performed for the removal of ammonia ligands in order to obtain finely dispersed rhodium metal on the carbon support surface. It can also be seen that an increase in the reduction temperature even to 500°C did not result in any agglomeration of metal particles (Fig. 6, curve *1*). It is believed that rhodium clusters in the calcined catalyst were stabilized by the formation of metal–support bonds, as evidenced by the presence of carbon in the nearest environment of rhodium atoms in this sample. However, the presence of ammonia ligands in the sample dried at 120°C and the absence of carbon from the nearest neighborhood of rhodium are favorable for the agglomeration of rhodium metal particles even at reduction temperatures of 250–350°C (Fig. 6, curve *2*). It is likely that the higher mobility of rhodium clusters in this sample was responsible for agglomeration, as found in [39].

### *Activity of the Rh/C(120) and Rh/C(350) Catalysts in Benzene Hydrogenation*

Figure 7 shows the temperature dependence of benzene conversion on the Rh/C(120) and Rh/C(350) catalysts prereduced at 350°C. It can be clearly seen that the activity of the Rh/C(350) sample was much higher than the activity of Rh/C(120). Thus, the conversion of benzene on the precalcined sample at 80°C was equal to 14%, whereas the dried sample was inactive at this temperature. Moreover, the conversion of benzene on Rh/C(350) over the temperature range 150–200°C was as high as 70–75%, whereas it was no higher than 10%

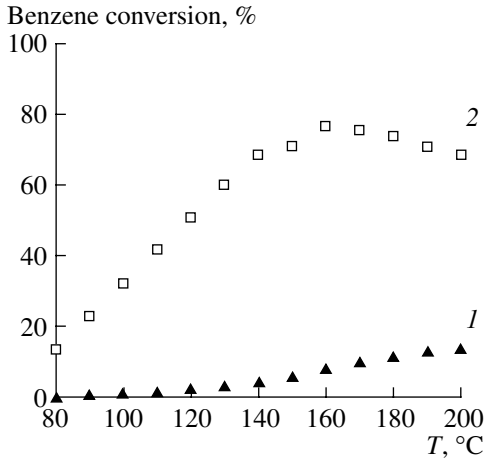


**Fig. 7.** Dependence of the conversion of benzene on the temperature of hydrogenation on the (*1*) Rh/C(120) and (*2*) Rh/C(350) catalysts.

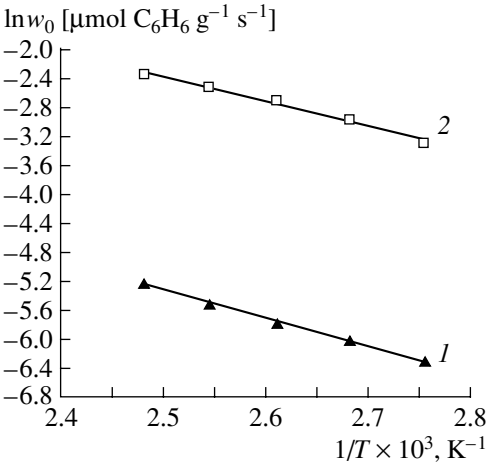


**Fig. 8.** Arrhenius plot of the rate of benzene hydrogenation on the (*1*) Rh/C(120) and (*2*) Rh/C(350) catalysts.

on the Rh/C(120) sample over the specified temperature range.

Figure 8 shows the temperature dependence of the rates of benzene hydrogenation on both of the Rh/C catalysts in the Arrhenius coordinates. It can be seen that the apparent activation energies of the reaction were similar over the test temperature range. The activation energies for the Rh/C(120) and Rh/C(350) catalysts were equal to 7.8 and 6.8 kcal/mol, respectively.

## CONCLUSIONS

The following conclusions can be drawn based on the experimental data: In the initial calcined sample, rhodium occurs in a six-coordinated state, which is typical of trivalent rhodium. In the uncalcined sample, the coordination number of rhodium is closer to 5. The EXAFS data suggest that $NH_3$ ligands constitute the major portion of the environment of rhodium in this sample. The presence of these ligands somewhat increases the positive charge on the rhodium atom, as compared with the uncalcined sample.

The reduction of the uncalcined Rh/C(120) catalyst begins at 200°C and results in the formation of coarse metal particles. The size of these particles continues to decrease as the reduction temperature is increased to 500°C. The absence of carbon atoms from the nearest environment of rhodium is indicative of the absence of the direct interaction of rhodium with the support. In turn, this results in the rapid agglomeration of metal particles upon the loss of ammonia ligands and reduction.

The reduction of the sample precalcined at 350°C in air begins even at 100°C and results in the formation of highly dispersed metal particles. The presence of carbon atoms as the nearest neighbors of the rhodium atom is favorable for conservation of fine rhodium particles as the reduction temperature is increased up to 500°C.

In turn, difference in the dispersity of rhodium particles in the calcined and uncalcined samples is responsible for differences in the rates of benzene hydrogenation. At the same temperature, the conversion of benzene into cyclohexane is much higher (by a factor of 15–20) on the sample containing small rhodium particles. Similar apparent activation energies of the reaction over both of these catalysts imply that the difference between reaction rates on the low-dispersity Rh/C(120) and high-dispersity Rh/C(350) samples is due mainly to differences in the surface areas of rhodium metal accessible to reaction, rather than to changes in the reaction mechanism.

## ACKNOWLEDGMENTS

This study was performed within the framework of a contract between the Zelinskii Institute of Organic Chemistry, Russian Academy of Sciences, and the HASYLAB at DESY (project no. I-02-013).

## REFERENCES

1. Stiles, A.V., *Catalyst Supports and Supported Catalysts: Theoretical and Applied Concepts*, Stoneham: Butterworths, 1987, p. 107.
2. Keim, W., *Catalysis in $C_1$ Chemistry*, Dordrecht: Reidel, 1983.
3. Roth, J.F., Craddock, J.H., Hersman, A., and Paulik, F.E., *Chem. Tech.*, 1971, p. 600.
4. Schultz, R.G. and Montgomery, P.D., *Am. Chem. Soc., Div. Pet. Chem.*, 1972, vol. 17, p. 13.
5. Robinson, K.K., Hersman, A., Craddock, J.H., and Roth, J.F., *J. Catal.*, 1972, vol. 27, p. 289.
6. Howard, M.J., Jones, M.D., Roberts, M.S., and Taylor, S.A., *Catal. Today*, 1993, vol. 18, p. 325.
7. Fujimoto K., Omata K., Shikada T., Tominaga H., *ACS. Symp. Ser.*, 1987, vol. 28, p. 208.

8. Rylander, P.N. and Steele, D.R., *Engelhard Ind. Tech. Bull.*, 1962, vol. 3, p. 91.
9. Freidlin, L.Kh. and Popova, I.L., *Izv. Akad. Nauk SSSR, Ser. Khim.*, 1972, vol. 4, p. 905.
10. Freidlin, L.Kh., Litvin, E.F., Yakubenok, V.V., and Pivonenkova, L.P., *Izv. Akad. Nauk SSSR, Ser. Khim.*, 1973, vol. 4, p. 850.
11. Skell, P.S. and Ahmed, S.N., *J. Catal.*, 1990, vol. 125, p. 525.
12. Bragin, O.V., Olfer'eva, T.G., Preobrazhenskii, A.V., Liberman, A.L., and Kazanskii, B.A., *Dokl. Akad. Nauk SSSR*, 1972, vol. 202, p. 339.
13. Bernas, A., Kumar, N., Mäki-Arvela, P., Kul'kova, N.V., Holmbom, B., Salmi, T., and Murzin, D.Yu., *Appl. Catal., A*, 2003, vol. 245, p. 257.
14. Ukisu, Y. and Miyadera, T., *Chemosphere*, 2002, vol. 46, p. 507.
15. Kulkarni, P.P., Deshmukh, S.S., Kovalchuk, V.I., and d'Itri, J.L., *Catal. Lett.*, 1999, vol. 61, p. 161.
16. Yunusov, S.M., Kalyuzhnaya, E.S., Moroz, B.L., Agafonova, S.N., Licholobov, V.A., and Shur, V.B., *Appl. Catal., A*, 2001, vol. 218, p. 251.
17. Halttunen, M.E., Neimela, M.K., Krause, A.O.I., Vaara, T., and Vuori, A.I., *Appl. Catal., A*, 2001, vol. 205, p. 37.
18. Halttunen, M.E., Neimelä, M.K., Krause, A.O.I., and Vuori, A.I., *Appl. Catal., A*, 1999, vol. 182, p. 115.
19. Kainulainen, T.A., Neimelä, M.K., and Krause, A.O.I., *J. Mol. Catal. A: Chem.*, 1999, vol. 140, p. 173.
20. Kainulainen, T.A., Neimelä, M.K., and Krause, A.O.I., *J. Mol. Catal. A: Chem.*, 1997, vol. 122, p. 39.
21. Sakagami, H., Ohta, N., Endo, S., Harada, T., Takanashi, N., and Matsuda, T., *J. Catal.*, 1997, vol. 171, p. 449.
22. Schultz, R.G. and Montgomery, P.D., *J. Catal.*, 1996, vol. 109, p. 105.
23. Takahashi, N., Takabatake, Y., Sakagami, H., Imizu, Y., Okazaki, N., and Tada, A., *J. Catal.*, 1996, vol. 159, p. 491.
24. Halttunen, M.E., Neimela, M.K., Krause, A.O.I., and Vuori, A.I., *J. Mol. Catal. A: Chem.*, 1996, vol. 109, p. 209.
25. Yamasaki, K., Uchimoto, T., Kakuta, N., and Ueno, A., *J. Mol. Catal.,* 1988, vol. 48, p. 21.
26. Takanashi, N., Takeyama, T., Yanagibashi, T., and Takada, Y., *J. Catal.*, 1992, vol. 136, p. 531.
27. Stakheev, A.Yu., Baeva, G.N., Telegina, N.S., Volynsky, A.B., Kustov, L.M., and Minachev, Kh.M., *Mendeleev Commun.*, 2000, vol. 2, p. 99.
28. Shpiro, E.S., Tuleuova, G.J., Zaikovsky, V.I., Vasina, T.V., Tkachenko, O.P., Bragin, O.V., and Minachev, Kh.M., *Stud. Surf. Sci. Catal.*, 1989, vol. 46, p. 142.
29. Sachtler, W.M.H. and Stakheev, A.Yu., *Catal. Today*, 1992, vol. 12, p. 283.
30. Kampers, F.W.H., Maas, T.M.J., van Grondelle, J., Brinkgreve, D.C., and Koningsberger, D.C., *Rev. Sci. Instrum.*, 1989, vol. 60, p. 2635.
31. Klementiev, K.V., *VIPER for Windows (Visual Processing in EXAFS Researches)*, www.desy.de/~klmn/viper.html.
32. Ankundinov, A.L., Ravel, B., Rehr, J.J., and Conradson, S.D., *Phys. Rev.*, 1998, vol. 58, p. 7565.
33. Borowski, M., *J. Phys.*, 1997, vol. 4, no. 7, p. 2.
34. Kochubei, D.I., Shitova, N.B., and Nikitenko, S.G., *Kinet. Katal.*, 2002, vol. 43, no. 4, p. 601.
35. Pinxt, H.H.C.M., Kuster B.F.M., Koningsberger D.C., and Marin, G.B, *Catal. Today*, 1998, vol. 39, no. 4, p. 351.
36. Ros, T.G., Keller, D.E., van Dillen, A.J., Geus, J.W., and Koningsberger, D.C., *J. Catal.*, 2002, vol. 211, no. 1, p. 85.
37. Ros, T.G., Keller, D.E., van der Lee, M.K., van Dillen, A.J., Geus, J.W., and Koningsberger, D.C., *J. Mol. Catal. A: Chem.*, 2002, vol. 186, nos. 1–2, p. 13.
38. Koningsberger, D.C., Mojet, B.L., van Dorssen, G.E., and Ramaker, D.E., *Top. Catal.*, 2000, vol. 10, p. 143.
39. Zou, W. and Gonzales, R.D., *J. Catal.*, 1992, vol. 133, p. 202.